A terahertz view on magnetization dynamics

Awari, Nilesh

CHAPTER 6

THz-Driven Spin Excitation in High Magnetic Fields: Case of NiO

In this chapter we focus on the study of the THz driven response of spin waves in antiferromagnetic (AFM) NiO. The AFM mode of NiO is excited with high intensity THz pulses which are resonant with the AFM mode, and probed with the Faraday rotation technique involving femtosecond laser pulses. At the beginning of the chapter, we introduce the importance of studying the dynamical properties of AFM mode for advance high frequency spintronics applications. The implemented experimental scheme is then discussed. The theory of AFM resonance is discussed in brief. In the later phase of the chapter, the temperature and the field dependence of the observed AFM mode in NiO in the vicinity of 1 THz are discussed. The measurements reveal two antiferromagnetic resonance modes which can be distinguished by their characteristic magnetic field dependencies. The observed field dependence of the AFM mode at different temperatures is discussed on the basis of an eight-sublattice model. Our study indicates that a two-sublattice model is insufficient for the description of spin dynamics in NiO, while the magnetic-dipolar interactions and magneto-crystalline anisotropy play important roles.

This chapter is based on the publication:
Wang, Zhe, et al. "Magnetic field dependence of antiferromagnetic resonance in NiO." Applied Physics Letters 112, 25 (2018)

6.1 Introduction

The fundamental understanding of how fast the magnetic state of a material can be manipulated for future data storage applications has driven the field of antiferromagnetic (AFM) based spintronics devices [1, 2]. The absence of macroscopic magnetization makes AFM-based devices preferred candidates for robust memory storage applications, rapid switching and manipulation of spins [3–5]. Also as AFM response (magnon mode) has higher resonant frequencies than ferromagnetic resonance (FMR), it makes them prime candidates for high frequency spintronics devices. One of the most promising AFM compounds for device fabrication is Nickel Oxide (NiO) as it is easy to grow in the form of bulk single crystals as well as in nano-films [6–10]. The magnon mode in NiO has been shown to be at 1 THz. Current research on NiO focuses on investigating interesting phenomena, such as the THz magnon dynamics [11] and the Spin Hall magneto-resistance [12]. In a recent experiment on NiO, coherent control and manipulation of magnon mode was demonstrated [5, 13]. For the development of spintronics devices operating at higher frequencies, it is important to understand how to manipulate and control the magnetization state at ultra-fast time scales ($\sim$ 100 fs).

NiO has been studied extensively because of its simpler crystal structure as compared to other antiferromagnetic materials. NiO is a prototype antiferromanget with a Néel temperature of 523 K. Above the Néel temperature, NiO crystallizes in a centrosymmetric cubic structure of NaCl while below the Néel temperature to rhombohedral structure by contracting in one of the four <111> axes. This contraction, as shown in Ref.[14], takes place due to exchange striction resulting in the formation of four equivalent crystallographic twin domains. Neutron diffraction experiments have shown that the easy axis for Ni^{2+} spins lies in the {111} plane [14, 15] and the spin direction is shifted by 180° in adjacent planes (Figure 6.1). The magnetic moments are ferromagnetically aligned on the {111} plane and they antiferromagnetically couple with the magnetic moments in neighboring {111} planes. The predominant spin interaction is an AFM exchange between the next nearest neighbor Ni^{2+} ions, which are linked by a super-exchange path of the 180° Ni^{2+}-O^{2-}-Ni^{2+} configuration. Due to additional magnetic anisotropy, the spins are oriented along one of the three $<11\bar{2}>$ axes, which corresponds to three equivalent spin domains in each crystallographic domain [16].

The low-energy dynamic properties of the NiO spin degrees of freedom are characterized by antiferromagnetic spin-wave excitations as revealed by inelastic neutron scattering [14]. They were explained based on a two-sublattice antiferromagnetic model [14, 15, 17]. Further experimental studies, especially based on Raman and Brillouin spectroscopy, revealed five antiferromagnetic magnon modes close to zero wave vector [18, 19], thereby

suggesting the magnetic structure should to be more complex than a two-sublattice antiferromagnet. These observations were satisfactorily explained by an eight-sublattice model [18], which has been further extended to study the dependence of the three lowest-lying modes (below 0.5 THz) on an external magnetic field by Brillouin spectroscopy [20].

So far, however, it has remained unclear how the two highest-lying modes would evolve in an external magnetic field. Experimentally, one high-energy mode at $\sim$ 1 THz has recently been shown to be coherently controllable by intense THz electromagnetic pulses at room temperature [13]. Here, taking advantage of a new type of narrow-band tunable superradiant THz source [21], we selectively excite these resonances and measure their frequency as a function of temperature and magnetic field. While at room temperature, only one antiferromagnetic spin resonance mode with a nonlinear dependence on the external magnetic field is present, an additional mode appears below 250 K which exhibits a much weaker field dependence. Calculations based on an eight-sublattice model of the spin interactions in NiO were performed [18, 20], which can describe the observed field dependencies of the two high-frequency antiferromagnetic spin resonance modes.

6.2 Experimental details

In order to selectively excite the AFM mode in NiO and to study its dynamics, the narrow band THz pump Faraday rotation probe technique was employed. Narrow-band THz pulses generated at the TELBE facility [21], centered at 1 THz, were used to selectively excite the magnon mode. Probe pulses were generated from a Ti:sapphire laser system with 100 fs pulse duration. The measurement of spin deflection is obtained by recording the rotation of probe polarization utilizing Faraday effect. The schematic of the experimental set up is shown in Figure 6.2. The electric field profile of the 1 THz pump and its frequency spectrum is shown in Figure 6.3. The THz pump has a maximum electric field of $\sim$ 60 kV/cm with 20 % bandwidth. 1 THz pump pulses were focused on a 50 μm thick free standing NiO with collinear probe pulses. The change in probe polarization was measured with a pair of balanced photo-diodes. By varying the time delay between pump and probe pulses, we determined the dynamics of the AFM state. The measurements were also done at varying temperatures from 3 K to 280 K along with external fields up to 10 T in a commercial Oxford Instrument split coil magnet. The magnetic field was applied parallel to the incident laser beam and perpendicular to a (111) surface of a single crystalline NiO sample. For this field orientation, the Ni moments within the different antiferromagnetic domains remain stabilized along the $< 11\bar{2} >$ directions in finite fields.

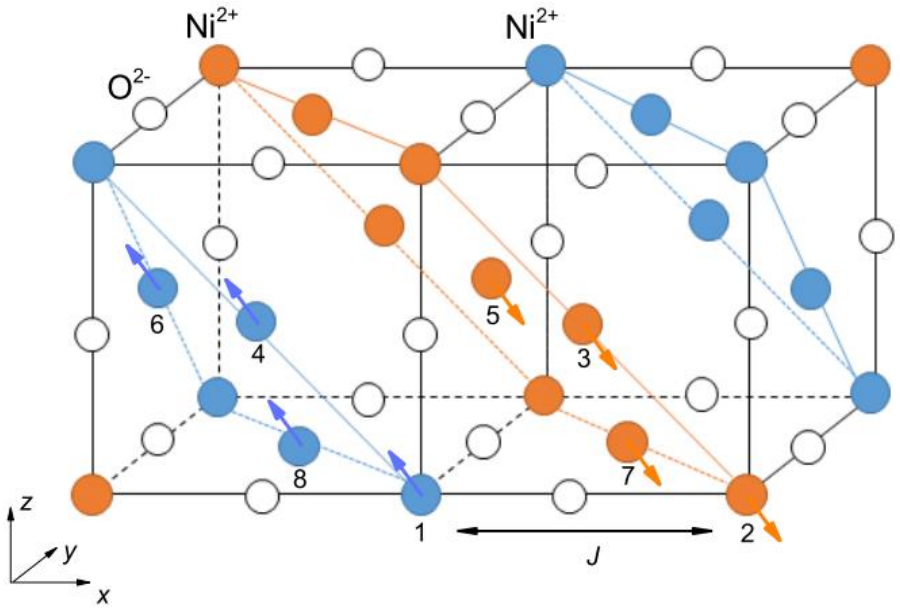

FIGURE 6.1: Illustration of the crystallographic and magnetic structure of NiO, based on an eight sub-lattice model. Antiferromagnetic structure consists of ferromagnetically aligned spins along the (111) planes which are alternatively stacked along the perpendicular direction. Spins of the Ni^{2+} ions are along the $<11\bar{2}>$ directions, as indicated by the arrows. The dominant spin interaction is the super-exchange between the next-nearest-neighbor Ni^{2+} ions via the 180° Ni^{2+}-O^{2-}-Ni^{2+} configuration as denoted by J.

The AFM mode in antiferromagnetic material can be explained in general, using the two sub-lattice model, by the theory of Keffer and Kittel [22]. In typical antiferromagnetic materials one has two sub-lattices with magnetization $\boldsymbol{M_1}$ and $\boldsymbol{M_2}$. The equation of motion for the two magnetizations are given by the following equations,

$$\frac{d\boldsymbol{M_1}}{dt} = -\gamma\left[\boldsymbol{M_1} \times \left(\boldsymbol{H_0} + \boldsymbol{H_A} - \lambda \boldsymbol{H_2}\right)\right] \tag{6.1}$$

$$\frac{d\boldsymbol{M_2}}{dt} = -\gamma\left[\boldsymbol{M_2} \times \left(\boldsymbol{H_0} - \boldsymbol{H_A} - \lambda \boldsymbol{H_1}\right)\right] \tag{6.2}$$

here, $\boldsymbol{H_0}$ is the static magnetic field, $\boldsymbol{H_A}$ is the uniaxial anisotropy, and $\boldsymbol{H_{exch\ 1,2}} = \lambda M_{2,1}$ is the exchange field. The anisotropy field acts on two sub-lattices in the opposite direction. If $\boldsymbol{H_0}$ and $\boldsymbol{H_A}$ are parallel and in the $\hat{z}$ direction, then the resonance

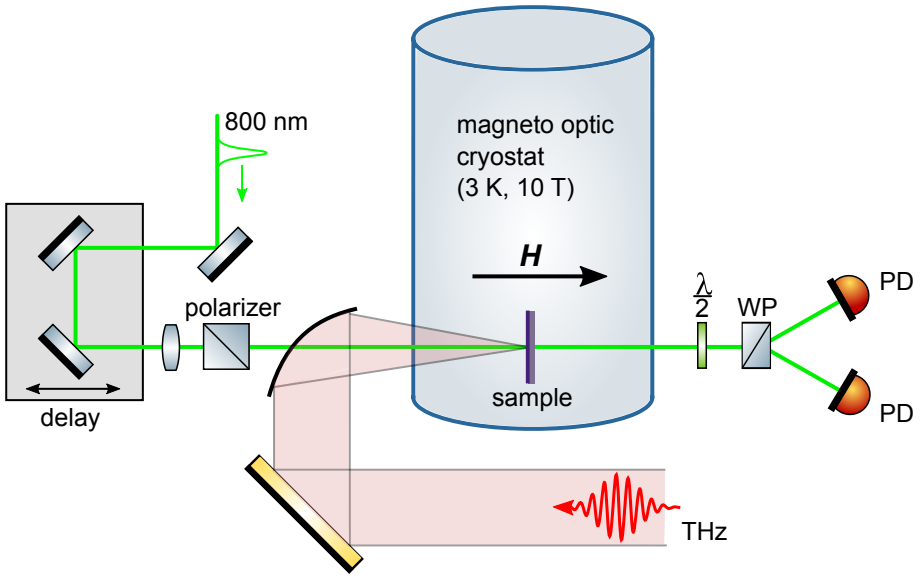

FIGURE 6.2: Sketch of the THz pump Faraday rotation probe technique equipped with a cryomagnet up to 10 T field. The THz pulses (red) are focused on the sample at normal incidence. 800 nm probe pulses (green) are collinear with THz pulses. The transient change in the magnetization of the sample is probed by the Faraday rotation of the probe polarization with a timing accuracy of 12 fs. $\frac{\lambda}{2}$, WP and PD are the half-wave plate, the Wollaston prism and the photo-diodes respectively.

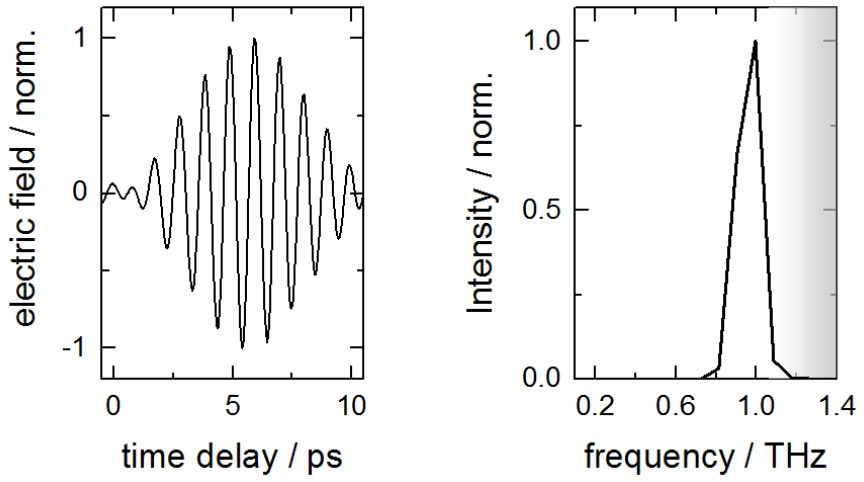

FIGURE 6.3: (a) Time domain signal of the 1 THz multi-cycle pump pulse. (b) Power spectrum of the pump pulse obtained by Fourier transformation. Above 1.1 THz the signal is strongly suppressed by water absorption.

frequencies are as given below [17],

$$\omega_{\mathrm{res}} = \pm\gamma H_0 \pm \gamma\left[H_{\mathrm{A}}\left(2H_{\mathrm{E}} + H_{\mathrm{A}}\right)\right]^{\frac{1}{2}} \tag{6.3}$$

Equation 6.3 shows that even for zero external field, there is a finite frequency of AFM mode, determined by the exchange and anisotropy fields. In the absence of an external field, the motion of magnetization is governed by four frequency modes which can be grouped into two distinct modes as depicted in Figure 6.4.

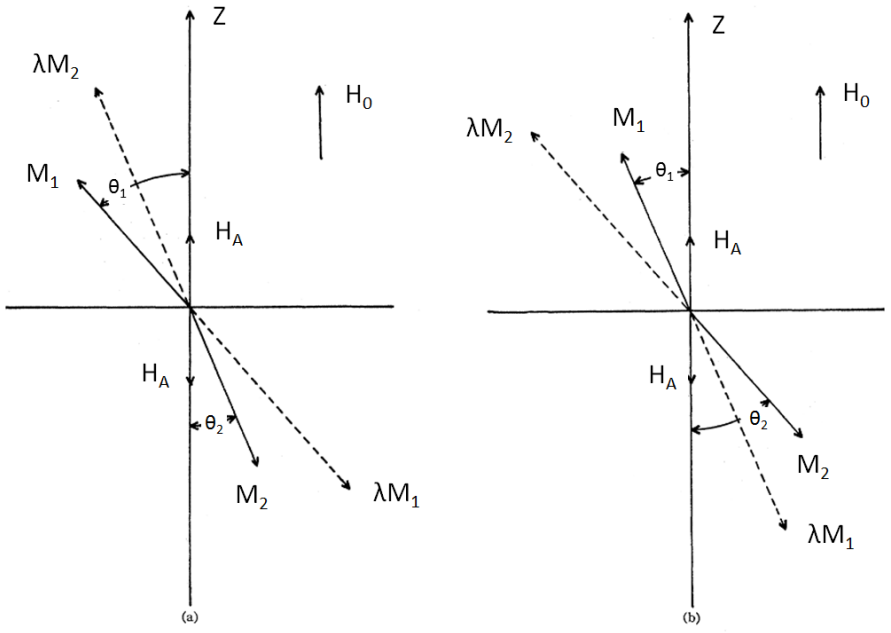

FIGURE 6.4: Illustration of the two distinct magnetic modes in antiferromangetic resonance. H_0 the is static magnetic field, $M_{1,2}$ is the magnetization of the two sublattices of the antiferromagnetic material, H_A is the uniaxial magnetic anisotropy. Figure adapted from [22]

Both of the magnetizations rotate around the effective magnetization, determined by the axis of an uniaxial anisotropy field. Observing from the positive $\hat{z}$ direction, both modes either rotate in clockwise or anti clockwise direction, as shown in Figure 6.4(a). The same holds true for the other two modes as depicted in Figure 6.4(b). The only difference between these two modes is the stiff cone angle $\eta = \theta_2/\theta_1$. For modes shown in Figure 6.4(a), η is smaller than 1, whereas for modes shown in Figure 6.4(b) it is larger than 1. The η is a material dependent property given by Ref. [22].

$$\eta = \left[H_{\mathrm{A}} + H_{\mathrm{E}} + (H_{\mathrm{A}}(2H_{\mathrm{E}} + H_{\mathrm{A}}))^{1/2}\right] \Big/ H_{\mathrm{E}} \tag{6.4}$$

Here H_A is the anisotropy field and H_E is the exchange field. When the external field H_0 is applied, the resonance frequency of one mode increases by the factor $\gamma\mu_0 H_0$, while it decreases by same amount for the other mode. This model, based on two sub-lattices, fails to explain the five distinct AFM modes observed in NiO [18, 19]. These observations were satisfactorily discussed in the context of an eight-sublattice model [18], which has been further extended to study the field dependence of the three lowest-lying modes (below 0.5 THz) observed by Brillouin spectroscopy in an external magnetic field [20]. So far it remains unclear how the two highest-lying modes would evolve in an external magnetic field, although experimentally one high-energy mode has been proven to be coherently controllable by intense THz electromagnetic fields at room temperature. Here, using the TELBE facility, one excites the AFM mode resonantly. The THz magnetic field and electron spins interact via Zeeman torque and collectively excite the magnon mode, as discussed in reference [23].

$$\boldsymbol{\tau} = \gamma \boldsymbol{S} \times \boldsymbol{B}_{\mathrm{THz}} \tag{6.5}$$

Here, γ is the gyro-magnetic constant for electron spin $\boldsymbol{S}$ and $\boldsymbol{B}_{\mathrm{THz}}$ denotes the magnetic field component of the THz transient. The projection of the induced magnetization $\mathbf{M}(\mathrm{t})$ along the propagation direction ($\mathbf{e_k}$) of the NIR probe causes circular birefringence and rotates the probe polarization by an angle

$$\theta_{\mathrm{F}}(t) = Vl < \boldsymbol{e_k}.\boldsymbol{M}(t) > \tag{6.6}$$

where V is the Verdet constant of the material and l is a distance travelled by the NIR probe inside the material.

6.3 Results & Discussion

6.3.1 Temperature dependence of AFM mode

Figure 6.5a shows the recorded Faraday rotation time scan for NiO at 280 K without external field and in the air. The FFT of the time scans (Figure 6.5b) shows the $\sim$ 1 THz mode which corresponds to the high frequency spin (AFM) mode in NiO. The observed time trace of Faraday rotation is free from any background heating as usually observed in all-optical pump probe techniques. In Figure 6.5a, we see the beating effect which can be understood as the superposition of the 1 THz AFM mode and a water

absorption line present at around 1 THz, which lies within the bandwidth of the THz pump.

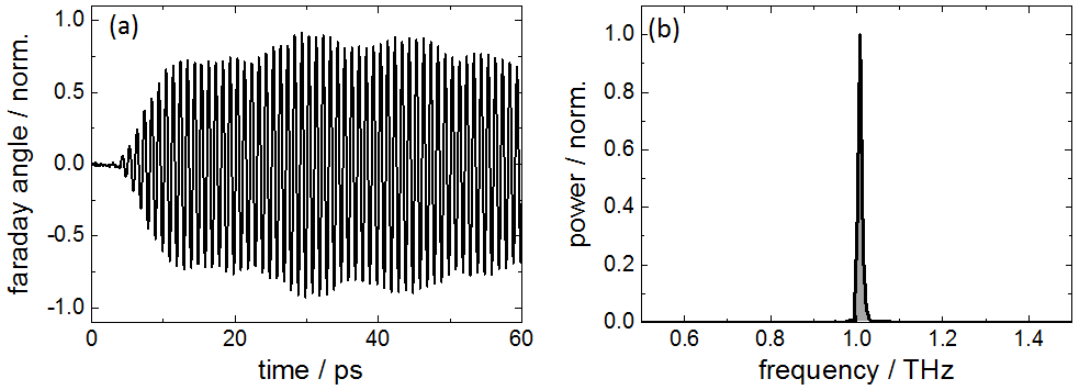

FIGURE 6.5: Typical transient Faraday measurement for NiO obtained at 280 K. The coherent oscillation of the magnetization is probed by the determination of the polarization change. (a) Time domain trace of the Faraday rotation at room temperature. (b) Power spectrum of the Faraday rotation signal.

The measurements of the temperature dependence at zero field have been performed for various temperatures between 3.3 and 280 K [see Figure 6.6(a)]. At each temperature, the amplitude spectrum derived from Fourier transformation of the transient Faraday signal exhibits a single peak with a well-defined position. The peak positions are shown in Figure 6.6(b) as a function of temperature with the error bars indicating the full width at half maximum (FWHM) of the peaks. With decreasing temperature from 280 K, the peak position shifts to higher frequencies monotonically. This hardening of the peak frequency is consistent with previous measurements of the temperature dependence [24], which reflects an increase in the spontaneous magnetization of each sublattice with decreasing temperature [22]. It is worth noting that in our experiment, the higher-frequency components are affected by water absorption lines. Thus, for the low-temperature measurements, the obtained resonance frequencies have larger uncertainty. The 1.29 THz mode, observed by Raman spectroscopy at low temperatures [19], was not observed because this mode can not be resonantly pumped by the THz pump at 1 THz with 20 % bandwidth.

The observed temperature dependence of the AFM mode in NiO can be explained by equation [25, 26],

$$\frac{T}{T_{\mathrm{N}}} = F(\sigma)\left[1 + 6S^2\sigma^2\frac{j}{J}\right] \tag{6.7}$$

where $F(\sigma) = -3Nk_{\mathrm{B}}S\sigma\left[(S+1)(\delta S^*/\delta\sigma)T\right]^{-1}$, N is the total amount of the spin, $\mathrm{k_B}$ is the Boltzmann constant, J is the exchange interaction constant, j/J defines the

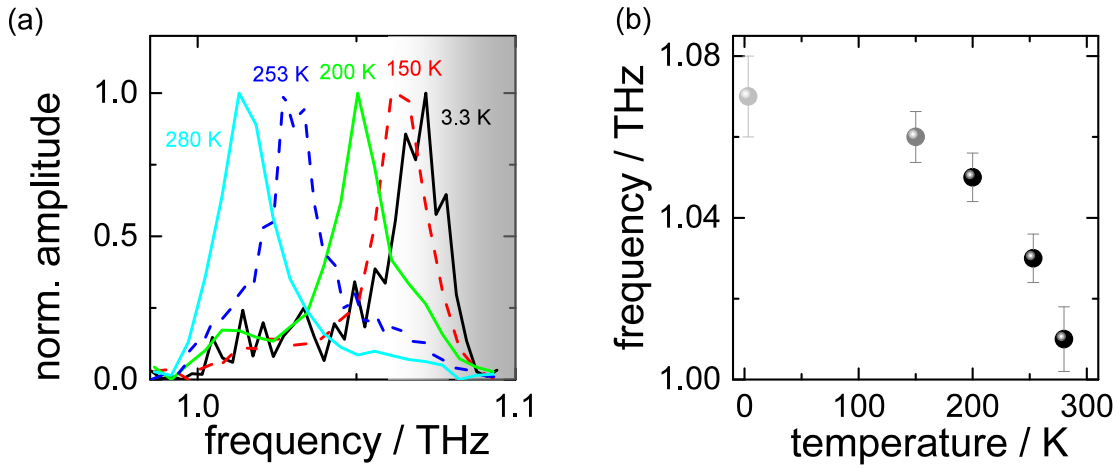

FIGURE 6.6: Temperature dependence of the magnon mode in NiO. (a) Amplitude spectra obtained from Fourier transformation of the time-domain signals of Faraday rotation angle at various temperatures. The shaded area in the high-frequency limit indicates the spectral range where the THz radiation is strongly reduced by water absorption. (b) Temperature dependence of the peak frequencies in (a). Error bars indicate the apparent full widths at the half maxima.

magnitude of the exchange interactions, S is the total spin angular momentum of the system under consideration, S^* is the spin entropy of the system under consideration and σ is normalized magnetization M/M_0 with M_0 being magnetization at 0 K.

6.3.2 Field dependence of AFM mode

The THz-pump Faraday-rotation probe experiments have been extended to study the effects of external magnetic fields at different temperatures. Figure 6.7 shows the field dependence of zero field frequency mode at three different temperatures. The zero field mode shifts to higher frequencies with increasing external field and decreasing temperature. Figures 6.7a, 6,7b, and 6.7c show the obtained amplitude spectra in various applied magnetic fields up to 10 T at 280 K, 253 K, and 200 K, respectively. At 280 K, the peak position of the single peak continuously shifts to higher frequencies with increasing magnetic fields. The frequencies at the peak positions are shown in Figure 6.7b, which clearly exhibit a nonlinear increase with increasing external magnetic field. Such a nonlinear field dependence has been predicted for antiferromagnets in which an in-plane anisotropy is also important in addition to the uniaxial anisotropy. In contrast, at 253 K and 200 K, a second peak appears for magnetic fields above 6 T. While the observed peak position is plotted as a function of applied magnetic field [Figure 6.7 (b,d,f)], the higher frequency mode exhibits non-linear dependence on applied filed where as the other mode is almost field independent. It is worth noting that at zero field, Raman spectroscopy has also revealed two modes at low temperatures, consistent with our observations.

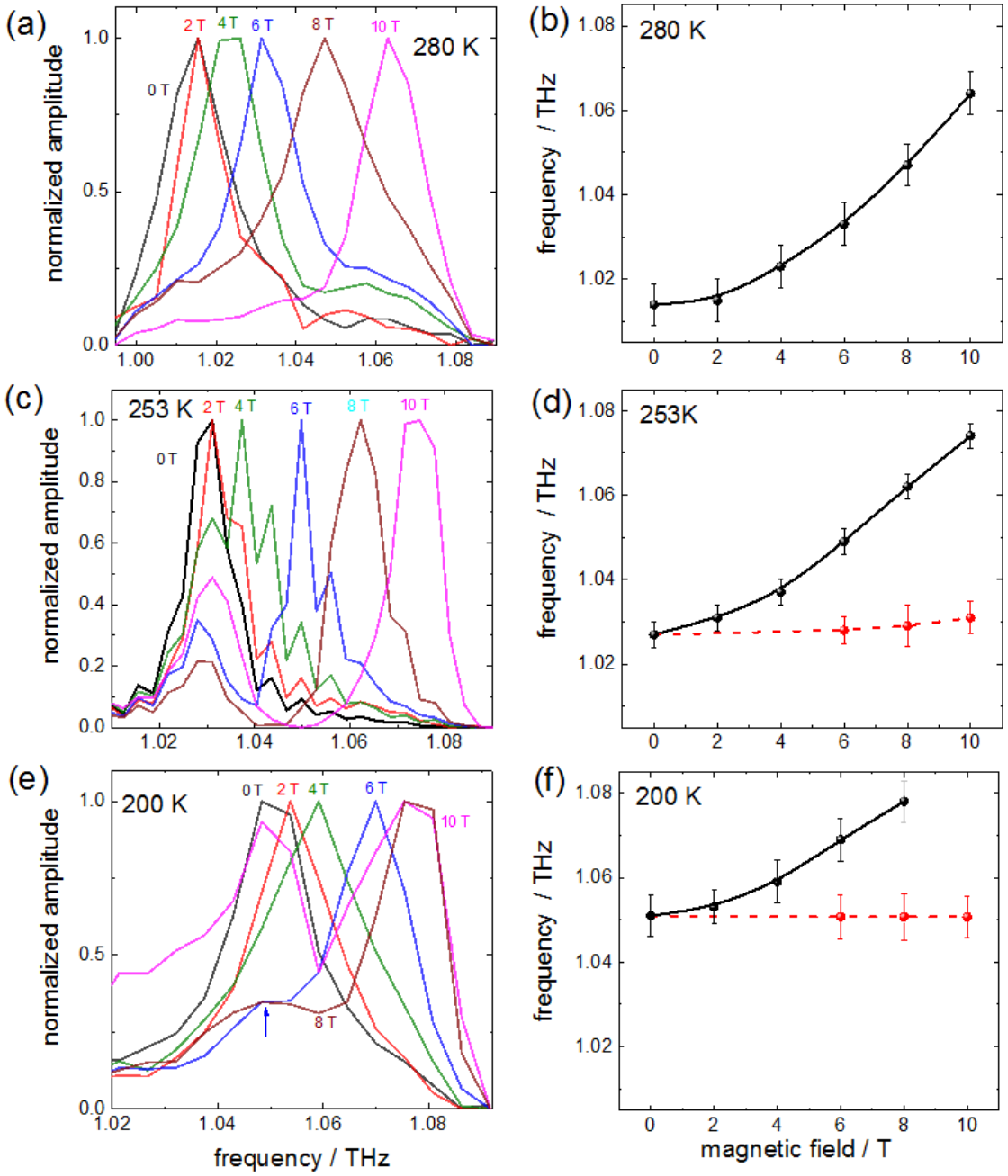

FIGURE 6.7: Magnetic field dependence at (a,b) 280 K, (c,d) 253 K and (e,f) 200 K. While only one mode is observed at 280 K, at the lower temperatures two modes are resolved. The qualitatively different field-dependencies of the two modes are in agreement with the predicted behaviors for mode A and mode B (see Figure 6.8 and Eq.(6.8)). In (b,d,f), the solid lines are guides for the eyes.

To understand the field-dependent behavior, our collaborators performed calculations of an eight-sublattice model, as described in Ref. [18, 20]. In contrast to the common two-sublattice model [14, 15], which cannot explain our observations, we show that the eight-sublattice model correctly predicts not only the two antiferromagnetic modes around 1 THz, but also their characteristic field dependencies. In the eight-sublattice model, the magnetic interactions comprise the antiferromagnetic exchange interactions E_{exch}, magnetic-dipole interactions E_{dip}, magnetic anisotropy E_{ani}, and a Zeeman interaction with an external magnetic field E_{Zeeman},

$$E = E_{\mathrm{dip}} + E_{\mathrm{exch}} + E_{\mathrm{ani}} + E_{\mathrm{Zeeman}} \tag{6.8}$$

The exchange energy term is given by,

$$E_{\mathrm{exch}} = J\big(\boldsymbol{m_1}\cdot\boldsymbol{m_2} + \boldsymbol{m_3}\cdot\boldsymbol{m_4} + \boldsymbol{m_5}\cdot\boldsymbol{m_6} + \boldsymbol{m_7}\cdot\boldsymbol{m_8}\big) \tag{6.9}$$

with J being the antiferromagnetic coupling constant. The exchange energy term couples only the sublattices 1 and 2, 3 and 4 , 5 and 6, and 7 and 8.

E_{dip} can be written as,

$$E_{\mathrm{dip}} = D\sum_i \left[\sum_{j>i} \boldsymbol{m_i}.T_{\mathrm{ij}}.\boldsymbol{m_j}\right] \tag{6.10}$$

The magnitude of D is exclusively determined by the magnetic moment of each Ni atom and lattice constant, -4×10^4 erg/cm^3. The dipole energy term defines the coupling between four AF lattices in ferromagnetically aligned (111) planes, but it does not account for alignment of spins in any preferred axis in this plane. In order to do so the magneto-crystalline anisotropy term is introduced as follows,

$$E_{\mathrm{ani}} = K\sum_i (m_{\mathrm{ix}}m_{\mathrm{iy}}m_{\mathrm{iz}})^2 \tag{6.11}$$

The magneto-crystalline constant $K < 0$ favors spins aligning along the <111> directions. A compromise with the stronger dipolar interactions leads to the orientation of spins close to the $[11\bar{2}]$ direction. This anisotropy favors alignment along <111> directions, which acts in the opposite sense to the dipolar term. In order to model the experimentally observed frequencies, the magnitude of K necessarily is small and has a small effect on the (111) easy planes [18].

In addition to this, the externally applied magnetic field interacts with each sublattice with the Zeeman term as shown below.

$$E_{\text{Zeeman}} = -g\mu_B \boldsymbol{H} \cdot \sum_i \boldsymbol{m}_i \tag{6.12}$$

The equilibrium values corresponding to the eight sub-lattices are found by direct minimization of the free-energy density given in equation (6.9). The magnetization of each sub-lattice is given by,

$$m_i = ((\sin\theta_i \cos\phi_i), (\sin\theta_i \sin\phi_i), (\cos\theta_i)) \tag{6.13}$$

Here polar coordinates are used to define the magnetization of the sub-lattice with θ_i being the polar angle of the magnetization with respect to Z axis which is normal to the surface of NiO, and ϕ_i is the azimuth angle in the surface plane. Following references[27, 28], a matrix is constructed from the second derivatives of the energy $E_{\theta(\phi)i\phi(\theta)j}$ with respect to magnetization angles θ_i and ϕ_j, in which the matrix elements $B_{n,m}$ are given by [20],

$$B_{2i-1,2j-1} = E_{\theta(i)\phi(j)} / \sin\theta_j \tag{6.14}$$

$$B_{2i,2j-1} = E_{\phi(i)\phi(j)} / \sin\theta_i \, \sin\theta_j \tag{6.15}$$

$$B_{2i,2j} = -E_{\phi(i)\theta(j)} / \sin\theta_i \tag{6.16}$$

$$B_{2i-1,2j} = -E_{\phi(i)\theta(j)} \tag{6.17}$$

By solving eigenvalues d_k of the matrix, frequencies of the antiferromagnetic modes are obtained as $\omega_k = i\gamma d_k / M$,

where γ is the gyro-magnetic ratio ($98\, cm^{-1}/Oe$ for Ni) [29] and M is the saturation magnetization of each sublattice $M = \mu_B / a^3 = 128\, G$.

This model, essentially focusing on the zero-temperature spin dynamics, has successfully described the experimentally observed modes by Raman and Brillouin spectroscopy at the lowest temperatures [20], and the field dependencies of the three lower-lying modes [18]. According to this model, application of a high external magnetic field ($H > 2$ T) can lead to the instability of the spin domains in most situations. For example, if the external magnetic field is applied along the spin orientation of one spin domain, i.e. $H \parallel [11\bar{2}]$, the zero-field magnetic structure becomes unstable above ~ 1 T. A quite stable configuration is found for the external field applied along the [111] direction, which is exactly the orientation of a crystallographic domain that is perpendicular to the sample surface [23]. In this case, the spins are stabilized to be oriented along the

$<11\bar{2}>$ directions, meaning that the zero-field spin configuration remains stable at high fields. Thus, our theoretical results are intrinsic to a single spin domain, which are presented in Figure 6.8 for the two higher-lying modes (i.e. 1.29 THz and 1.15 THz), where $J = 8.36 \times 10^8$ erg/cm^3, $D = -4.4 \times 10^4$ erg/cm^3, $K = 9 \times 10^4$ erg/cm^3, and the value of Lande g-factor for the spin Ni^{2+} ions is taken as 2 [14, 20]. While the 1.15 THz mode is almost field-independent up to 10 T, because the oscillating sub-lattice magnetizations of this mode have larger components along the $<1\bar{1}0>$ directions which is perpendicular to the applied field. In contrast, the 1.29 THz mode evidently shifts to higher frequencies with increasing magnetic field.

Upon Comparison with the experimental observations, there is agreement on the field dependencies of the two resonance modes. Naturally we assume that the thermal excitations [15] do not qualitatively alter the dependencies on an external magnetic field. Thus, we can assign the mode with nonlinear field dependence as the mode A of 1.29 THz obtained from the model calculation (see Figure 6.8), while the other mode, observed at 253 and 200 K and almost field-independent up to 10 T (see Figure 6.7 and Figure 6.8), should correspond to the mode B of 1.15 THz. It should be noted that the agreement between eight sub-lattice model calculations and the experimental observations is a qualitative one. In order to have quantitative agreement between them, one needs to do the theoretical calculations at finite temperatures. With the current 0 K calculations it is possible to adjust the free parameter and overlay calculations on the experimental observations but it does not give any additional information about the calculations.

6.4 Conclusion & Outlook

The coherent THz control of the AFM spin mode in NiO has been studied using superradiant THz radiation as a function of temperature and magnetic field. In high magnetic fields ($H > 6$ T) and at lower temperatures ($T \leq 253$ K), two different spin modes have been resolved with distinguished field dependencies. By performing calculations of an eight-sublattice model, the two modes are identified by their characteristic dependencies on the external magnetic fields. Thus, besides the antiferromagnetic exchange interactions of the Ni spins, our work has established that magnetic dipolar interactions and magneto-crystalline anisotropy are crucial for a proper description of the spin dynamics in the canonical antiferromagnet NiO. From an applied viewpoint, the existence of two modes with tunable frequency difference could open up new possibilities for control over antiferromagnetic order through individual or combined resonant pumping of the two modes. This work paves the way for studying non-equilibrium phenomenon driven by

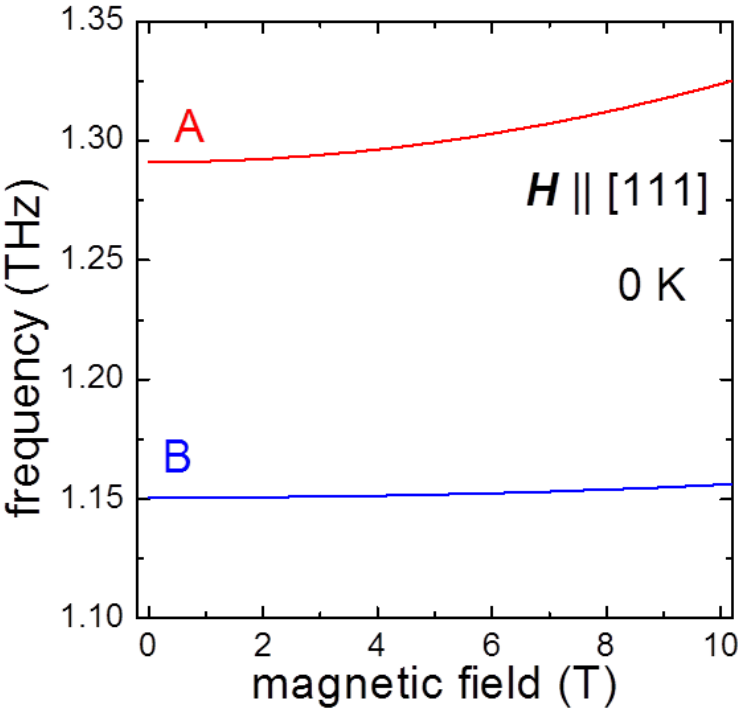

FIGURE 6.8: Field dependence of the higher-energy spin modes mode A at 1.29 THz (red) and mode B at 1.15 THz (blue) obtained from the eight-sublattice model [Eq. 6.8], for the external magnetic field applied along the [111] direction

intense THz fields at low temperatures and high magnetic fields based on high repetition rate superradiant sources.

6.5 Bibliography

[1] A. MacDonald and M. Tsoi, "Antiferromagnetic metal spintronics," *Philosophical Transactions of the Royal Society of London A: Mathematical, Physical and Engineering Sciences*, vol. 369, no. 1948, pp. 3098–3114, 2011.

[2] T. Moriyama, K. Oda, and T. Ono, "Spin torque control of antiferromagnetic moments in NiO," *arXiv preprint arXiv:1708.07682*, 2017.

[3] A. Kimel, A. Kirilyuk, A. Tsvetkov, R. Pisarev, and T. Rasing, "Laser-induced ultrafast spin reorientation in the antiferromagnet TmFeO3," *Nature*, vol. 429, no. 6994, p. 850, 2004.

[4] R. Gómez-Abal, O. Ney, K. Satitkovitchai, and W. Hübner, "All-optical subpicosecond magnetic switching in NiO (001)," *Physical review letters*, vol. 92, no. 22, p. 227402, 2004.

[5] N. Duong, T. Satoh, and M. Fiebig, "Ultrafast manipulation of antiferromagnetism of NiO," *Physical review letters*, vol. 93, no. 11, p. 117402, 2004.

[6] J. Stöhr, A. Scholl, T. Regan, S. Anders, J. Lüning, M. Scheinfein, H. Padmore, and R. White, "Images of the antiferromagnetic structure of a NiO (100) surface by means of x-ray magnetic linear dichroism spectromicroscopy," *Physical review letters*, vol. 83, no. 9, p. 1862, 1999.

[7] F. Hillebrecht, H. Ohldag, N. Weber, C. Bethke, U. Mick, M. Weiss, and J. Bahrdt, "Magnetic moments at the surface of antiferromagnetic NiO (100)," *Physical review letters*, vol. 86, no. 15, p. 3419, 2001.

[8] H. Ohldag, T. Regan, J. Stöhr, A. Scholl, F. Nolting, J. Lüning, C. Stamm, S. Anders, and R. White, "Spectroscopic identification and direct imaging of interfacial magnetic spins," *Physical review letters*, vol. 87, no. 24, p. 247201, 2001.

[9] S. Altieri, M. Finazzi, H. Hsieh, H.-J. Lin, C. Chen, T. Hibma, S. Valeri, and G. Sawatzky, "Magnetic dichroism and spin structure of antiferromagnetic NiO (001) films," *Physical review letters*, vol. 91, no. 13, p. 137201, 2003.

[10] A. Barbier, C. Mocuta, W. Neubeck, M. Mulazzi, F. Yakhou, K. Chesnel, A. Sollier, C. Vettier, and F. de Bergevin, "Surface and bulk spin ordering of antiferromagnetic materials: NiO (111)," *Physical review letters*, vol. 93, no. 25, p. 257208, 2004.

[11] T. Kohmoto, T. Moriyasu, S. Wakabayashi, H. Jinn, M. Takahara, and K. Kakita, "Observation of ultrafast magnon dynamics in antiferromagnetic nickel oxide by optical pump-probe and terahertz time-domain spectroscopies," *Journal of Infrared, Millimeter, and Terahertz Waves*, vol. 39, no. 1, pp. 77–92, 2018.

[12] G. R. Hoogeboom, A. Aqeel, T. Kuschel, T. T. Palstra, and B. J. van Wees, "Negative spin hall magnetoresistance of Pt on the bulk easy-plane antiferromagnet NiO," *Applied Physics Letters*, vol. 111, no. 5, p. 052409, 2017.

[13] T. Kampfrath, A. Sell, G. Klatt, A. Pashkin, S. Mährlein, T. Dekorsy, M. Wolf, M. Fiebig, A. Leitenstorfer, and R. Huber, "Coherent terahertz control of antiferromagnetic spin waves," *Nature Photonics*, vol. 5, no. 1, p. 31, 2011.

[14] M. T. Hutchings and E. Samuelsen, "Measurement of spin-wave dispersion in NiO by inelastic neutron scattering and its relation to magnetic properties," *Physical Review B*, vol. 6, no. 9, p. 3447, 1972.

[15] M. Cottam and A. L. Awang, "The effect of anisotropy on one-magnon light scattering from antiferromagnets. I. the antiferromagnetic region," *Journal of Physics C: Solid State Physics*, vol. 12, no. 1, p. 105, 1979.

[16] I. Sänger, V. V. Pavlov, M. Bayer, and M. Fiebig, "Distribution of antiferromagnetic spin and twin domains in NiO," *Physical Review B*, vol. 74, no. 14, p. 144401, 2006.

[17] C. Kittel, "Theory of antiferromagnetic resonance," *Physical Review*, vol. 82, no. 4, p. 565, 1951.

[18] J. Milano, L. Steren, and M. Grimsditch, "Effect of dipolar interaction on the antiferromagnetic resonance spectra of NiO," *Physical review letters*, vol. 93, no. 7, p. 077601, 2004.

[19] M. Grimsditch, L. McNeil, and D. Lockwood, "Unexpected behavior of the antiferromagnetic mode of NiO," *Physical Review B*, vol. 58, no. 21, p. 14462, 1998.

[20] J. Milano and M. Grimsditch, "Magnetic field effects on the NiO magnon spectra," *Physical Review B*, vol. 81, no. 9, p. 094415, 2010.

[21] B. Green, S. Kovalev, V. Asgekar, G. Geloni, U. Lehnert, T. Golz, M. Kuntzsch, C. Bauer, J. Hauser, J. Voigtlaender, *et al.*, "High-field high-repetition-rate sources for the coherent THz control of matter," *Scientific reports*, vol. 6, p. 22256, 2016.

[22] F. Keffer and C. Kittel, "Theory of antiferromagnetic resonance," *Physical Review*, vol. 85, no. 2, p. 329, 1952.

[23] T. Kampfrath, "T. kampfrath, a. sell, g. klatt, a. pashkin, s. mährlein, t. dekorsy, m. wolf, m. fiebig, a. leitenstorfer, and r. huber, nat. photonics 5, 31 (2011).," *Nat. Photonics*, vol. 5, p. 31, 2011.

[24] C. Kittel, *Introduction to Solid State Physics*. Wiley, 2005.

[25] M. Tinkham, "Far infrared spectra of magnetic materials," in *Proceedings of the Seventh Conference on Magnetism and Magnetic Materials*, pp. 1248–1253, Springer, 1962.

[26] D. Rodbell, I. Jacobs, J. Owen, and E. Harris, "Biquadratic exchange and the behavior of some antiferromagnetic substances," *Physical Review Letters*, vol. 11, no. 1, p. 10, 1963.

[27] Z. Zhang, L. Zhou, P. Wigen, and K. Ounadjela, "Angular dependence of ferromagnetic resonance in exchange-coupled Co/Ru/Co trilayer structures," *Physical Review B*, vol. 50, no. 9, p. 6094, 1994.

[28] J. Smit, "Ferromagnetic resonance absorption in $BaFe_{12}O_{19}$, a highly anisotropic crystal," *Philips Res. Rep.*, vol. 10, pp. 113–130, 1955.

[29] E. Wohlfahrt, "Ferromagnetic materials," *North-Holland Publishing, The Netherlands*, 1980.